

GEOG 471 Final Paper

Multi Sensor System Tracking an Oil Spill off
the Coast of Kuwait on August 2017

Group Members:
Noah Cameron
Ana Paula Diaz Garduno
Belle Tuen

April 9, 2023

Abstract

Many remote sensing techniques have been developed over the years to detect and monitor oil spills with SAR detection being the most common method due to its all weather capture ability and simple detection method. However, optical imagery and SAR imagery have different and complementary characteristics, this paper will look at how Sentinel-1, Sentinel-2, and Planetscope can work together to track an oil spill off the coast of Kuwait in 2017. Sentinel-1 was able to do initial detection using the SAR dark spot detection method as expected. The SAR detection method however was prone to overestimates and false positives. More research is needed before Sentinel-2 band ratios can help distinguish between look-alikes. Planetscope was used to fill in more of the temporal gaps wherever imagery is available. As a result all the sensors provided an accurate tracking of the oil spill movement through the dates of August 5th to the 16th showing that the oil moved north up the coast of Kuwait. A multi-sensor approach can provide major benefits in classifying false positives, filling in temporal gaps, and combined detection of both thick and thin oil.

Table of Contents

Abstract	ii
List of Tables	v
1 Introduction	1
2 Methodology	2
2.1 Study Area	2
2.2 Datasets	2
2.2.1 Planetscope Data	3
2.2.2 Sentinel-1 Data	4
2.2.3 Sentinel-2 Data	5
2.3 Analysis	6
2.3.1 Sentinel-1 Analysis	6
2.3.2 Sentinel-2 Analysis	8
2.3.3 Planetscope Analysis	10
3 Results	11
3.1 Sentinel-1	11
3.2 Sentinel-2 Band Ratios and False Colour Composites	11
3.3 Sentinel-2 Classification Results	18
3.4 Planetscope	18
3.5 Classification Based on Combined Results	22
4 Discussion	23
4.1 Planetscope Limitations	23
4.2 Sentinel-1 Discussion	25
4.2.1 Uncertainties and Drawbacks	25

4.2.2	SNAP OS Detection	27
4.3	Sentinel-2 Band Ratios	27
4.4	K-Means Clustering	30
4.5	Ideal Oil Spill Multi-Sensor System Specifications	31
5	Conclusion	33
References		35

List of Tables

1	Satellites	4
2	Planetscope Datasets Used	4
3	Sentinel-1 Datasets Used	5
4	Sentinel-2 Datasets Used	5
5	Band Details for Sentinel-2	9
6	Input Parameters for the Rayleigh Correction Tool in SNAP	9

List of Figures

1	Map of study area and nearby features	3
2	Diagram describing the methodology for each sensor	6
3	Comparison of dark spot in Sentinel-1 images vs dark spot raster extracted by dark spot detection.	12
4	Zoomed in dark spot detection via Sentinel-1 shows overestimation where areas of open water are classified as small clusters of oil.	13
5	True colour image of the labelled oil slicks on Aug 11.	14
6	False colour image of the oil on Aug 11.	15
7	True Colour (A) and False Colour Composites (B,C,D) of oil on August 16	16
8	Individual band ratio responses for August 16	17
9	Transect Plot of Oil	17
10	Transect Plot of Cloud Shadow	19
11	True colour and False Colour composites on August 6th	19
12	K-means classification Results from Aug 11	20
13	K-means classification Results from Aug 16	21
14	Comparison of Planetscope true colour images vs oil spill extracted by eCognition.	22
15	The tracked path that the oil slick followed as detected from all sensors combined.	23
16	Total oil area measured over time by all sensors.	24
17	Left image shows results from k-means which classifies extra water as oil, Right image shows results from SNAP's OS Detection tool tutorial cop (2017), where some oil is not detected by the tool, and sticks out beyond the mask.	28

1 Introduction

Oil pollution adversely affects the marine environment (Renegar et al., 2022; Sardi et al., 2020) which is why one of UN's Sustainable Goals is to reduce marine pollution as target number 1 under goal 14 to “Conserve and sustainably use the oceans, seas and marine resources for sustainable development” (SDG, n.d.) Remote sensing has been used as a tool for the detection, estimation, and measurement of oil spills (Leifer et al., 2012; Al-Ruzouq et al., 2020). Many different techniques and approaches are done depending on the type of remote sensing data are used. The most common is Synthetic Aperture RADAR (SAR) data because it can capture data in all weather and at any time and for its ability to detect potential oil slicks (Alpers et al., 2017). Oil slicks appear as dark spots because the oil reduces the capillary waves and reduces backscattering in a process called Bragg Scattering (Leifer et al., 2012). For Bragg scattering to occur, there must be at least 2 m/s so enough contrast between the water and oil is present (Leifer et al., 2012). The common range of necessary wind is 2.09 to 8.33 m/s (Latini et al.) or 3.5 to 7 m/s (Garcia-Pineda et al., 2013). Other phenomenon (lookalikes) on the ocean's surface, like phytoplankton, algae films, grease, ship wakes, internal waves, also dampen the backscatter results (Al-Ruzouq et al., 2020). Distinguishing oil and lookalikes is the source of much research Al-Ruzouq et al. (2020). Dark spot detection methods (almost any segmentation approach based on SAR) are supported by lots of literature and have very low levels of uncertainty Capizzi et al. (2016). Identification and thickness estimates, however, have more uncertainties since thickness estimates have been only studied in labs. Passive optical imagery is also used for the detection and estimation of oil spills (Abou Samra and Ali, 2022; Rajendran et al., 2021a; ?; Leifer et al., 2012; Lu et al., 2013; Park et al., 2019; Schaeffer et al., 2022) however are limited due to the presence of clouds and the time of day. True colour imagery are used to visually classify the type of oil by the colour and the related thickness estimate with the Bonn Agreement Oil Appearance Code (Ivanov and Gerivani, 2021a). The colour of oil, however, is not reliably seen in true colour images because of sunglint conditions or sensor positioning and time of day (Park et al., 2019). Rajendran et al. (2021a), has studied the spectra of oil and water and coastal reefs to provide band ratios for Sentinel-2 imagery that can detect oil slicks that are not visible in true colour. This method is purely visualization and cannot estimate thickness.

Because optical imagery and SAR have different and often complementary characteristics, many studies include data from at least two different sensors in a multi sensor approach to track the progression of oil spills (Vankayalapati et al.; Mohammadi et al., 2021; Abou Samra and Ali, 2022; Zhao et al., 2014; Gafoor and Al Shehhi, 2022). They rely on SAR data and use the optical imagery for a more continual view of the oil spill. The

oil features are most commonly extracted by image segmentation and object based image analysis for both types of data ([Kolokoussis and Karathanassi; Karantzalos and Argialas, 2008](#); [Mohammadi et al., 2021](#); [Park et al., 2019](#)). This research will explore how SAR from Sentinel-1 and optical imagery from Sentinel-2 and Planetscope can be used to track an oil spill off the coast of Kuwait in 2017 in a multi sensor approach. While Planet data is limited in that there are no data beyond 15 kilometers off the coast and the georeferenced accuracy over the water is questionable ([Schaeffer et al., 2022](#)), the daily revisit time can, in theory, aid in tracking the oil close to the coast ([Vankayalapati et al.](#)). The objectives of this study are to detect dark oil slicks and estimate oil thickness with Sentinel-1, visualize the oil spill through Sentinel-2 band ratios, test a pixel-based approach to extract oil slick features, and use Planet and OBIA in Ecognition to study the coastal oil slicks. The expectation is that oil slick detection will be easier with Sentinel-1 results than with sentinel-2 and Planet. The pixel-based classification will yield mediocre and noisy results. The band ratios from [Rajendran et al. \(2021a\)](#) will create visualizations of the oil slicks and Planet will show the progression of the oil across the coast.

2 Methodology

2.1 Study Area

The Persian Gulf is a hotspot for oil slicks ([Dong et al., 2022](#)) due to a high concentration of oil offshore development including crude oil pipelines linking platforms with onshore refineries, and oil transportation ([Sardi et al., 2020](#)). All countries with coasts to the Persian Gulf, Iran, Iraq, Saudi Arabia, Qatar, Kuwait, are major exporters and producers of oil and therefore there is a high rate of pollution ([Evtushenko et al., 2019](#); [Zhao et al., 2014](#)). The oil spill that was analyzed in this study was reported on the 10th of August 2017, off the southern coast of Kuwait in the Persian Gulf. The oil spill extent is shown in Figure 1. On August 11th, the oil reached the beaches of the resort community Al Khain ([Press, 2017](#)). The source of the oil spill was not reported but it is speculated it was from an oil pipe leak due to the construction for Al Zour refinery, Kuwait's largest refinery which started operations in 2019 ([Calcuttawala, 2017](#)).

2.2 Datasets

Data were collected from three different satellites, Sentinel-1, Sentinel-2, and Planetscope, for the multi-sensor approach. Each satellite was picked to maximize spatial, temporal

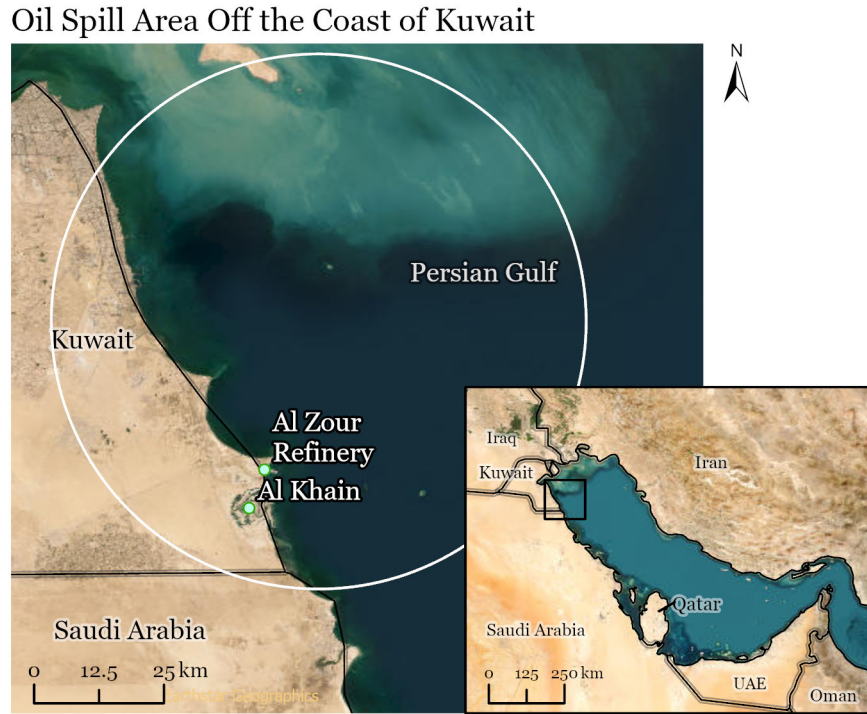


Figure 1: Map of study area and nearby features

and spectral resolutions for the most comprehensive view of the oil spill. Table 1 is a comparison between each.

2.2.1 Planetscope Data

To enhance the possibility of filling in the temporal gap between Sentinel-1 and Sentinel-2, Planetscope was chosen due to the close to daily revisit time on the constellations. This would be very useful in tracking the oil spill since it can help cover days where the Sentinel-1 and Sentinel-2 do not have images. Moreover, according to Schaeffer et al. (2022) Planetscope has possible potential for oil spill detection that not many papers have explored yet. The last reason Planetscope was chosen was due to its high resolution that allows the images to visually contain smaller oil slicks and spills. Detection would be less important for very big oil spills since it would be really easy to detect due to the sheer volume of the spill, but for initial detection, small oil spills tend to be forgotten and go by

Table 1: Satellites

Satellite	Spatial Resolution	Temporal Resolution	Spectral Resolution
Sentinel-1 IWS (Interferometric Wide Swath)	5m x 20m	Revisit time of ~5 days	VV Polarization
Sentinel-2 MSI (Multispectral Instrument)	20m x 20m	Revisit time of ~5 days	13 bands in the Visible, NIR and SWIR
Planetscope	3m x 3m	Daily	4 bands (red, green, blue, NIR)

undetected. The images used in this project from Planetscope were all taken on the same day mosaicked together to fit the study area.

Table 2: Planetscope Datasets Used

Dataset Names	Date	Number of Images
20170811_070507_0c42	Aug 11, 2017	1
20170811_070507_1_0c42		
20170811_070506_0c42		
20170811_070508_0c42		

2.2.2 Sentinel-1 Data

Oil slick detection is heavily dependent on SAR data. Sentinel-1 was selected as the SAR data source since it provided the necessary “VV” polarization, “Ground Range Detected” product type ([Al-Ruzouq et al., 2020](#)), location, and time range for detecting the Kuwait oil slick. It also provided accessibility and ease of use in Google Earth Engine (GEE). A tool was created within GEE allowing for easy analysis of images to ensure that they were suitable for use before downloading. Next and Previous buttons were added and allowed for scrolling through the images that were available in the Kuwait area, within a specified date range. K-Means and Filter buttons also allowed for testing of k-means clustering and filtering methods on each image as well. The desired imagery was identified in GEE and then downloaded for further analysis from ESA Copernicus Open Access Hub. Data was not readily available but was easily requested and available for download within the next few hours.

Table 3: Sentinel-1 Datasets Used

Dataset Names	Date	Number of Images
S1A_IW_GRDH_1SDV_20170805T023856_20170805T023921_017782_01DCBB_3F82.zip	Aug 5, 2017	1
S1A_IW_GRDH_1SDV_20170810T024714_20170810T024738_017855_01DEF7_F48C.zip	Aug 10, 2017	1
S1A_IW_GRDH_1SDV_20170814T145031_20170814T145056_017921_01E0ED_82DF.zip	Aug 14, 2017	2
S1A_IW_GRDH_1SDV_20170814T145006_20170814T145031_017921_01E0ED_DB39.zip		

2.2.3 Sentinel-2 Data

The Sentinel-2 MSI mission was chosen to be part of the multi-sensor approach to tracking the oil spill because of the relatively high temporal and spectral resolution compared to Landsat (a candidate to the multi-sensor system) and Planet respectively. Since the oil spill occurred after Sentinel-2B was launched (March 2017), both satellites were used to reach a 5-day revisit time over the oil spill ([ESA](#)). The revisit time of Landsat would be too large, 16 days, for a phenomenon that changes daily. This permitted Sentinel-2 to contribute three days with oil spill data during the oil spill's progression. The different bands and their spatial and spectral details are in Table ???. The images were downloaded from the ESA Copernicus Open Access Hub, as well.

Table 4: Sentinel-2 Datasets Used

Dataset Names	Date	Number of Images
S2B_MSIL1C_20170806T071619_N0205_R006_T39RTM_20170806T072451.SAFE	Aug 6, 2017	1
S2A_MSIL1C_20170811T072301_N0205_R006_T39RTM_20170811T072308.SAFE	Aug 11, 2017	1
S2B_MSIL1C_20170816T072259_N0205_R006_T39RTM_20170816T072651.SAFE	Aug 16, 2017	2
S2B_MSIL1C_20170816T072259_N0205_R006_T39RTN_20170816T072651.SAFE		

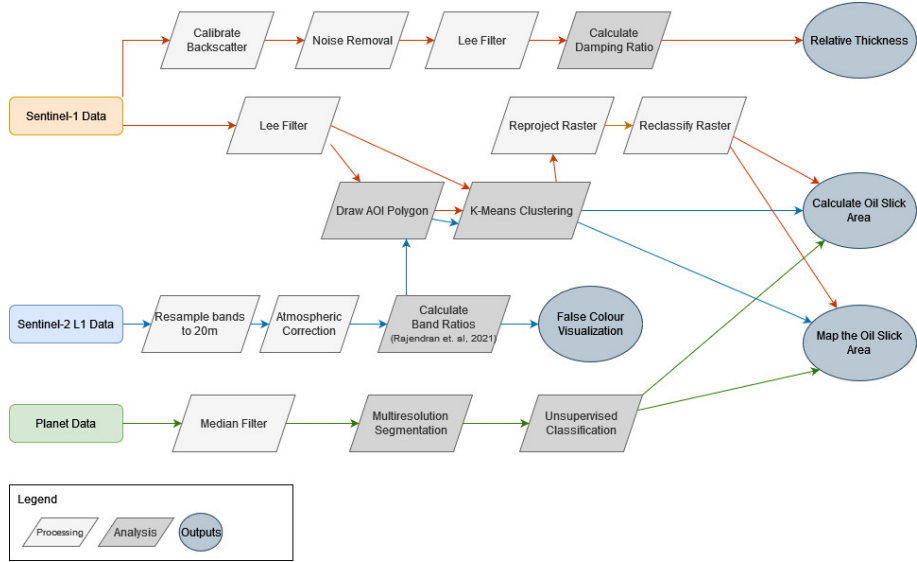


Figure 2: Diagram describing the methodology for each sensor

2.3 Analysis

Data from each sensor were subject to different preprocessing steps and analysis to estimate and map the oil spill area on each day and explained in the subsequent sections. The overall diagram of the analysis is demonstrated in Figure 2.

2.3.1 Sentinel-1 Analysis

Dark Spot Detection

To determine the oil slick area using Sentinel-1 imagery, the images were processed using SNAP as follows. First a 7x7 Lee filter was used to reduce speckle in the images. This was used because 7x7 windows showed the strongest reduction in speckle in a study comparing filtering methods by (Lee et al., 2009), while a review of oil spill detection studies found the Lee filter to be the most commonly used for oil spills Al-Ruzouq et al. (2020). The oil can be seen as dark spots after filtering, and an AOI polygon is drawn roughly around the oil area. The AOI polygon excludes land area if the oil is near a shoreline, to only include oil and water. Then k-means clustering classification was applied on the filtered image within the AOI polygon using 4 classes. The 4 classes were determined experimentally by testing different numbers of classes; this number could be changed based on the results. After the

k-means clustering, one of the identified classes can be marked as oil, while the rest are water. The resulting raster is then reprojected (reprojection tool in SNAP, reprojecting to any desired projection for GIS use), which allows for it to be added into ArcGIS Pro. In GIS, the raster is reclassified to only show the oil extent (oil layers were combined, and non-oil layers were deleted) and can be used to compare the oil area to the results from other dates and sensors. The total oil area was then calculated from this raster by calculating a new field in the attribute table, which multiplies the count of pixels by the resolution of each pixel (5m x 20m).

Dark Spot Classification

Dark spot detection is very accurate using Sentinel-1 relative to other sensors since oil is easy to see. Oil appears dark on a light background (water) due to dampened backscatter ([Al-Ruzouq et al., 2020](#)). The difficulty is that algal blooms, strong currents, or other look-alikes may also appear as dark spots. Many other papers classify these dark spots as oil or look-alikes by subjective factors: spots are likely to be oil if they are near a platform or ship, if they have a strong contrast to the open water, or if there is a lone dark spot surrounded by open water of non-varying colour ([Solberg et al., 1999](#)). Attempting to decide based on these criteria was inconclusive from experimentation, as it was still a judgment call, and dark spots could not be confidently categorized as oil or not. To increase confidence, other factors were also considered; dark spots were identified based on the location, size, and thickness relative to the known oil-slick areas that had already been detected. For example, if there was a dark spot on the 5th, and known oil on the 7th nearby, the size and thickness of the two would be compared. If it appeared that the volume of oil was similar (either similar area and thickness, or increased area with decreased thickness [spreading oil]) and would be on the correct path based on the oil's movement, the dark spot would be classified as the same oil. Another factor that was added was comparing to imagery without oil. For example, if there was a dark spot in a Sentinel-1 image, but no oil is seen in a Sentinel-2 image for the same date, the dark spot would be classified as a look-alike.

Relative Oil Thickness

Relative oil thickness was estimated for Sentinel-1 imagery by determining the damping ratios. The damping ratio is the average backscatter of the oil divided by the average backscatter of the open water. Although this ratio cannot determine an actual measurement of the oil depth, the ratio can be used to compare two oil slicks and see which is thicker ([Espeseth et al., 2022](#)) To determine the damping ratios, first, the imagery was processed in SNAP using backscatter calibration, used to convert digital numbers to backscatter values. Then, noise removal and Lee filtering were applied to reduce noise and speckle in the imagery. This process replicates the process of calculating damping ratios outlined by

[Caporusso et al. \(2022\)](#). Then a rough polygon was drawn to fit the thickest areas of the oil slick (darkest and most central), and a second polygon was drawn in the open water. This was digitized rather than using the dark spot detection areas, to focus only on how the thickest areas in the oil slick are changing over time. Using the statistics tool, the average pixel value was collected for each polygon, and the oil average was divided by the open water average to determine the damping ratio.

2.3.2 Sentinel-2 Analysis

Preprocessing

All preprocessing steps for the Sentinel –2 images were completed in SNAP. The images were downsampled to 20m in order to calculate band ratios between bands that are at 10 m and 20 m resolution later in the analysis. To downsample the 10m bands, the nearest input pixel value was set as the output pixel value. After resampling, the images were Rayleigh corrected to produce surface reflectance; level 1C images are top of atmosphere reflectance. Input parameters – sea level pressure in hPa, and estimated ozone thickness of the atmosphere in DU (Dobson Units) – were found at Columbia Climate School International Research Institute for Climate and Society Monthly Sea Level Pressure tool (Monthly Sea Level Pressure, n.d.) and at the Government of Canada’s Ozone Archive (Government of Canada, n.d.) for the month of August 2017. Table 6 contains the input parameters for each day. The sea level pressure was estimated to the closest isobar. The ozone thickness is reported in a range, so the mean value was used. The input parameters were different than the tool’s default. Additionally, subsets the regions of interest were mosaicked for the two images on August 16.

Analysis

Then, band ratios were calculated and added as new bands to the processed images. The Sentinel-2 band ratios were calculated by [Rajendran et al. \(2021a\)](#) and [Rajendran et al. \(2021b\)](#) to help distinguish oil spills in water. The band information are in Table 5. In total, 5 different ratios were calculated out of red, green, blue, red edge, near infrared, and shortwave infrared bands. Also, two different RGB false colour composites from these ratios have been used by multiple oil researchers to visualize oil ([Rajendran et al., 2021b](#); [Abou Samra and Ali, 2022](#); [Gafoor and Al Shehhi, 2022](#)). The same band ratios were calculated in this study however the ratio combination for the RGB colour composite that had the largest visual distinction was different in the red component, ratio B3/B2 instead of (B5+B6)/B7.

Table 5: Band Details for Sentinel-2

Band Name	Wavelength	Section of the EM Spectrum	Spatial Resolution
B1	443	Ultra Blue (Coastal and Aerosol)	60
B2	490	Blue	10
B3	560	Green	10
B4	665	Red	10
B5	705	Red-edge	20
B6	740	Near-Infrared	20
B7	783	Near-Infrared	20
B8	842	Near-Infrared	10
B8A	865	Near-Infrared	20
B9	945	Short wave Infrared (Atmospheric)	60
B10	1375	Short wave Infrared (Cirrus)	60
B11	1610	Short Wave Infrared	20
B12	2190	Short Wave Infrared	20

Table 6: Input Parameters for the Rayleigh Correction Tool in SNAP

Date	Sea Level Pressure (mB)	Ozone Thickness (du)
Aug 06, 2017	1002	287.7 (275-300)
Aug 11, 2017	1002	262.5 (250-275)
Aug 16, 2017	1002	287.7 (275-300)

An unsupervised classification, specifically k-means Clustering Analysis, was run to extract the oil pixels. Supervised classification was not used because of the lack of true ground data to use as training and testing data. Creating training and testing data points from the Sentinel-2 imagery to train a classifier was, also, not feasible due to the small sample size of visible oil pixels. The polygon of the region of interest of only areas with oil was created with the help of the false colour composite. The classification was only run on this area to reduce complexity and unnecessary clusters like land, clouds etc. The number of clusters was determined in an iterative manner. The result with the best visual overlap from the false colour composites to the classified oil was found to be 10 clusters. The seed, and other parameters were left as the default. The raster was exported as a geotiff and inputted into ArcGIS Pro to compare with other sensors and dates. The area calculation was done by multiplying the count of pixels by the area of a Sentinel-2 pixel (400 meters

squared).

2.3.3 Planetscope Analysis

Pre-Processing

Many of the literature used convoluted neural networks similar to Park et al. (2019)'s approach to do detection with Planetscope, however, due to the time constraints of this project, a different approach was taken in detecting oil slicks. Most of the analysis was done in eCognition with the final touches in ArcGIS Pro due to licensing restrictions on eCognition. Since Planetscope imagery needed to be mosaicked together to fit the study area, the images were first put into ArcGIS Pro to be exported as one file to make it easier to work with on eCognition. All Planetscope images that were used in this project were orthorectified with top of the atmosphere reflectance. The main pre-processing step done was to apply a median filter to help mitigate the sun glint in the imagery on top of generalizing the area to help smooth out the areas so it will be easier to segment in the next process.

Analysis

The main strength of eCognition is its ability to automatically extract and separate feature within the imagery. By using eCognition it is possible to do an unsupervised OBIA classification method to help detect common features within the image. The first step is segmentation using the Multiresolution Segmentation tool. This tool works by looking at every pixel and determining which pixel is its best fitting neighbour to segment with. If the pixels are mutually best-fitting with each other it is grouped together, otherwise it creates a new object. The parameters to determine the best-fitting neighbour is dependent on the scale, layer weights, colour, shape, compactness and smoothness. With a higher scale, shape, and smoothness the objects that are segmented come out bigger with more range in the pixel values and care more about how the object looked. With a higher colour and compactness, the objects are more segmented using the band pixel values and there are more objects than the other and are densely packed against each other. For this project, the NIR band was the most important so it was weighted 3 to 1 against the other bands. Moreover, for an oil spill it is most likely that the spill is a bigger shape covering a large area, so a more homogeneous look is better, therefore a higher scale was needed. After segmenting the areas, an unsupervised classification was done to obtain the objects that were similar in terms of band wavelengths only. This allowed the classification to extract likely objects that were likely to be oil just off of the band spectra and not care about the

shape of the object itself. Lastly, it is important to only colourize the oil classed objects so that it is possible to extract the oil areas as a vector.

Post-Processing

The methods above were done on the free trial version of eCognition which does not allow users to export the results. In order to work around this, a screenshot was taken of the results and put back into ArcGIS Pro. From there the screenshot was georeferenced again to the study area using the coast as the control points. To extract the resulting area as a vector, the screenshot is put through a k-means unsupervised classification that will group the oil class areas together. This can then be vectorized to get the oil slick area. The total area spilt can be calculated through the shape area of the vectorized oil spills or by calculating the number of pixels that match the RGB values of the coloured oil areas from the screenshot and multiplying it by the image resolution.

3 Results

3.1 Sentinel-1

The entirety of dark spots was extracted from Sentinel-1 dark spot detection as expected. The border of extracted shapes also matched the expected shape strongly. The conversion of Sentinel-1 into a raster representing the dark spot is shown in figure 3. Evidently, the shape of the raster (right-hand side) matches precisely with the expected dark spot (left side). However, the detection was prone to some overestimation. Many small clusters of open water have also been extracted as dark spots. Looking at the overall picture this is a small source of error that may not be noticed, but zooming in reveals how some patches of water are clearly misclassified figure 4. Despite this, the overall accuracy was still very strong.

3.2 Sentinel-2 Band Ratios and False Colour Composites

In Figure 5, there are couple of types of oil: black oil and grey oil sheens (labelled). Figure 6 shows the same extent but as a false colour composite of B3/B2, (B3+B4)/B2, (B11+B12)/B8. The oil sheens now look purple/blue like the water at the east end of the figure. And the black oil (labelled) is somewhat lost and not as visible. The oil in the south is clearer in the composite with a dark orange colour. Additionally, oil north of the

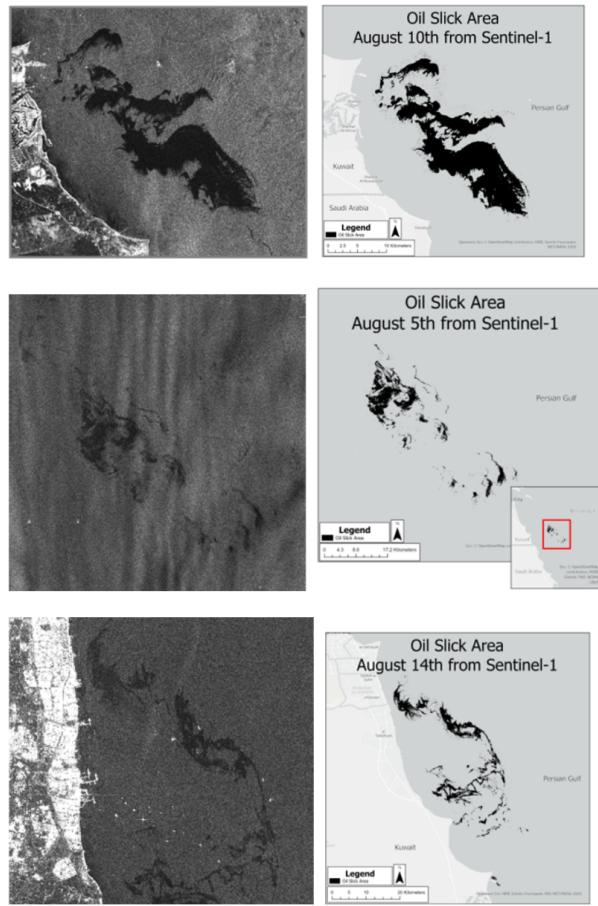


Figure 3: Comparison of dark spot in Sentinel-1 images vs dark spot raster extracted by dark spot detection.

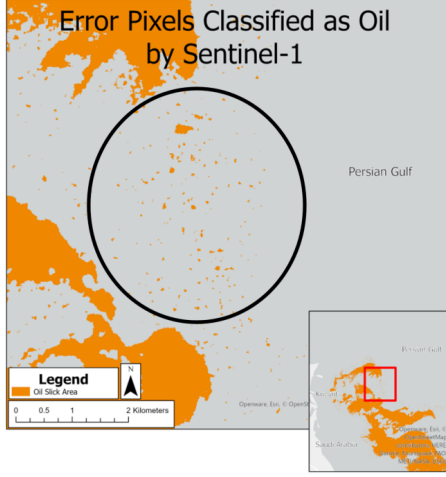


Figure 4: Zoomed in dark spot detection via Sentinel-1 shows overestimation where areas of open water are classified as small clusters of oil.

peninsula is now more visible since there is a higher contrast against the background water colour and a damped response from the light-coloured water in Figure 5.

The true colour mosaicked image for August 16, contains some clouds, thankfully mostly over land (Figure 7). The oil is practically imperceptible in this image (7A) and only visible in the false colour composites (7B, C, D). Land is visualized as white; green are the thick clouds while light purple are thin clouds, and its shadows are dark. The shallow water with suspended sediment goes from yellow to magenta with an increase in depth and distance from the river mouth (Rajendran et al., 2021a) The dark water is visualized mostly blue, and the oil slicks are the dark areas in the water. Figure 7C shows the oil in water with more sediment. The contrast is lower than in Figure 7D, but it is still perceptible. Figure 7D shows how clear the oil slicks appear.

Figure 8 contains the individual ratios that make up the false colour composite. The ratio that best visualizes the oil is the blue oil. The water's spectral response in the shortwave infrared is greater than the oil (Figure 9). There is a clear dip in the ratio meaning that the oil has less of a response in band 8 than the surrounding water. This, however, is very similar to the cloud shadows (Figure 10). Even though the profile plot for the cloud shadow shows a gradual decrease in the ratio compared to the stark differences in the oil profile plot, the values are still similar. Water is around 1.25-1.2, the oil response is around 1.1 and the cloud shadow spans from 1.1 to 1.0.

August 6th Results

True Colour Image on Aug.11 2017

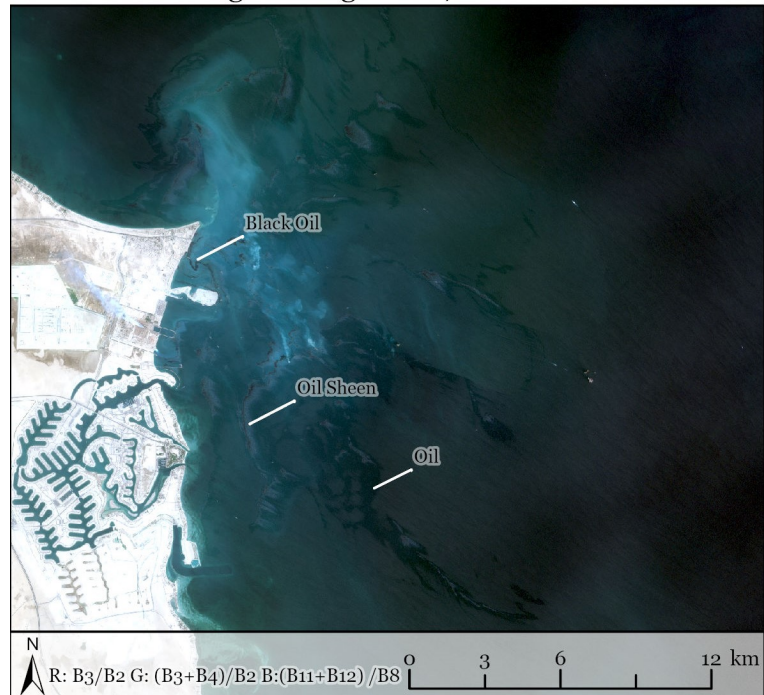


Figure 5: True colour image of the labelled oil slicks on Aug 11.

False Colour Subset of Sentinel-2 Imagery on Aug.11 2017

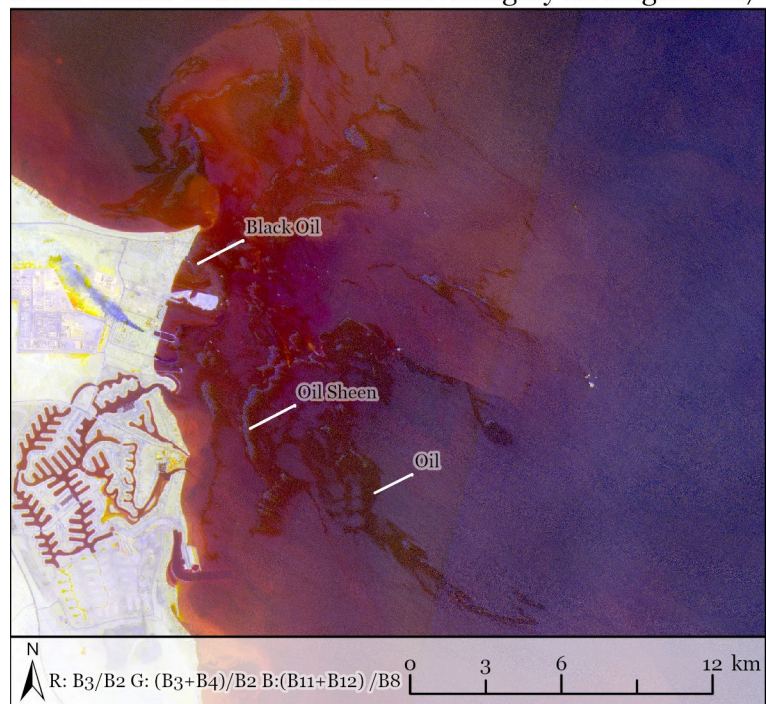


Figure 6: False colour image of the oil on Aug 11.

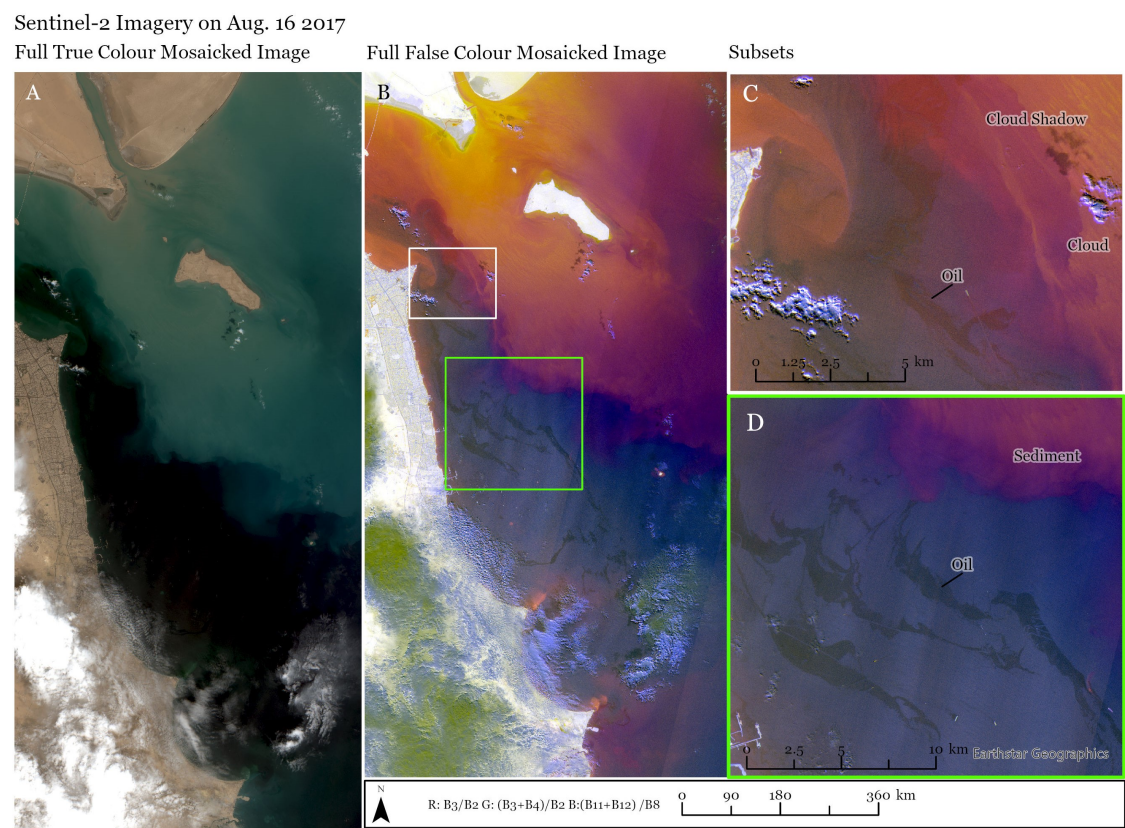


Figure 7: True Colour (A) and False Colour Composites (B,C,D) of oil on August 16

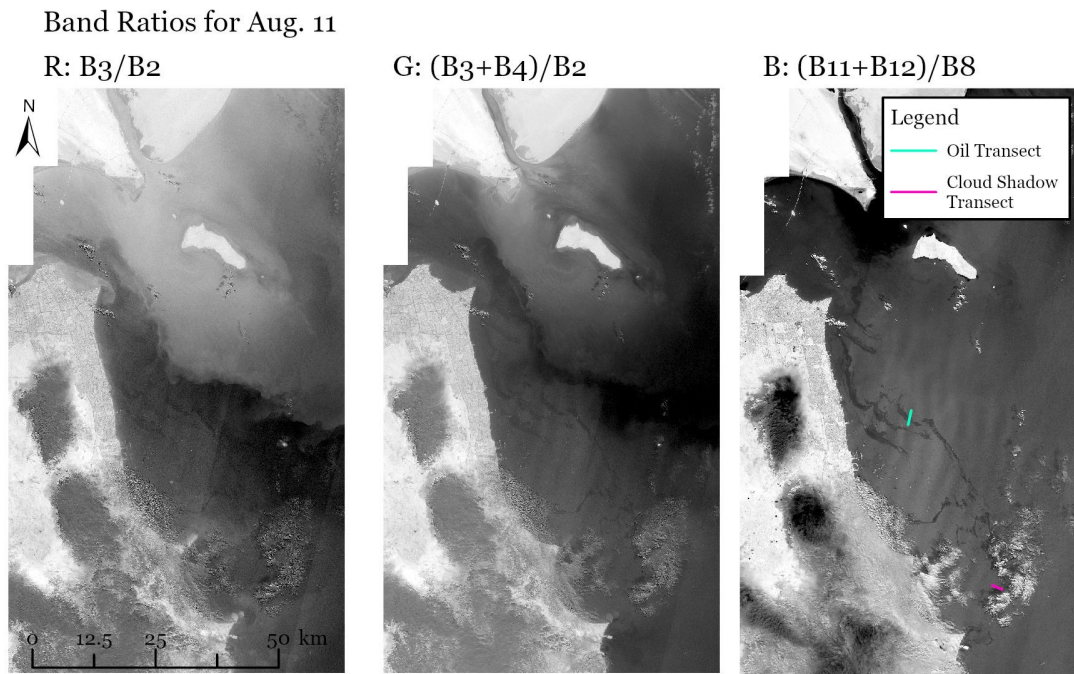


Figure 8: Individual band ratio responses for August 16

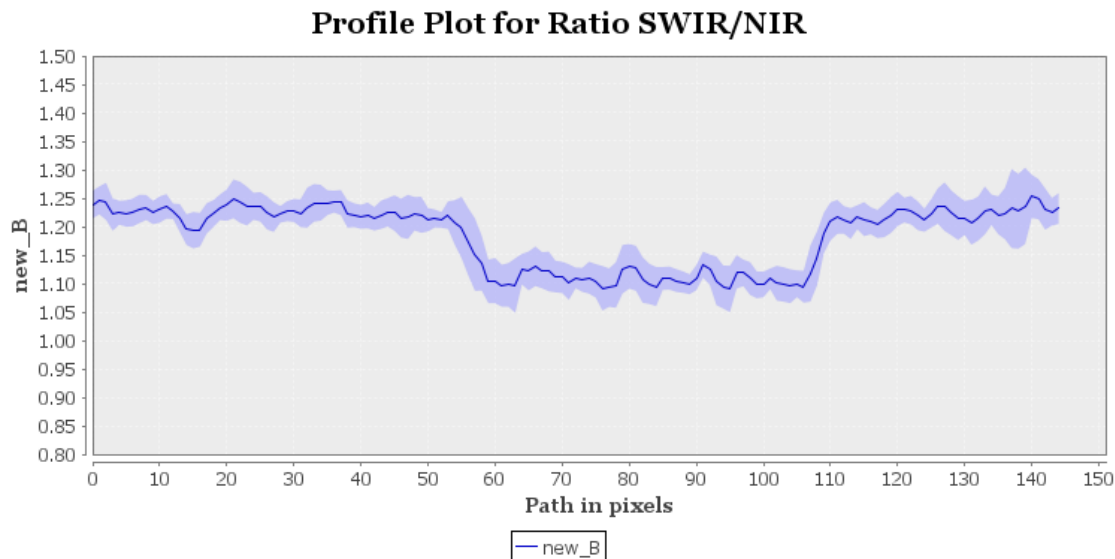


Figure 9: Transect Plot of Oil

The true colour and false colour composites for August 06 are shown in Figure 11. The bright yellow and orange near the coast represents sediment mixed with the water. The dark area farther out the coast may or may not be oil. Visual confirmation is inconclusive. More information in Section 4.2.1

3.3 Sentinel-2 Classification Results

The classification results were overlaid over the false colour composite to visually assess its accuracy. For August 11, two classes were used to display the oil, Figure 12. As seen in the zoomed-in section, there are many white misclassified pixels outside of the oil slick area. This can also be seen in the north section. There were also oil slicks that were not represented in the classification. The area circled by the black line in the zoomed-in map is an example of visible black oil in the true colour imagery that was not classified as oil. Also, within the oil slick area, there are pixels that are not classified as oil and should be resulting in a noisy classification with false positives and false negatives. Interestingly, the classification result for August 16 has less false positive errors in most of oil slick areas than August 11 (Figure 13). Nonetheless, the false positive errors mostly occurred in the northernmost section and near or at the cloud shadows (Figure 13B). In Figure 13A, the false negatives are to a minimum and the shape of the oil slick was classified correctly. Even the clean streaks left by the boats were classified correctly. However, the oil pixels within the oil slick area are a little sparse because of the false positive pixels.

3.4 Planetscope

The image on the left of Figure(14) shows the true colour composite of the study area that was available on Planetscope. The black lines on the top left are streaks of oil that can be confirmed visually along with the streaks in the middle that are being pushed by waves moving north-west. The image on the right of Figure(14) shows the area that was detected as oil by eCognition. ECognition managed to detect the areas that had thicker oil by using the 4 bands from Planetscope. While it is hard to determine the accuracy of this image since there is no information about this oil spill, it is safe to say the area is overall correct when taking the Sentinel-2 August 11th detection image into account. The shape, location, and overall area of the spill was in accordance with the Sentinel-2 image.

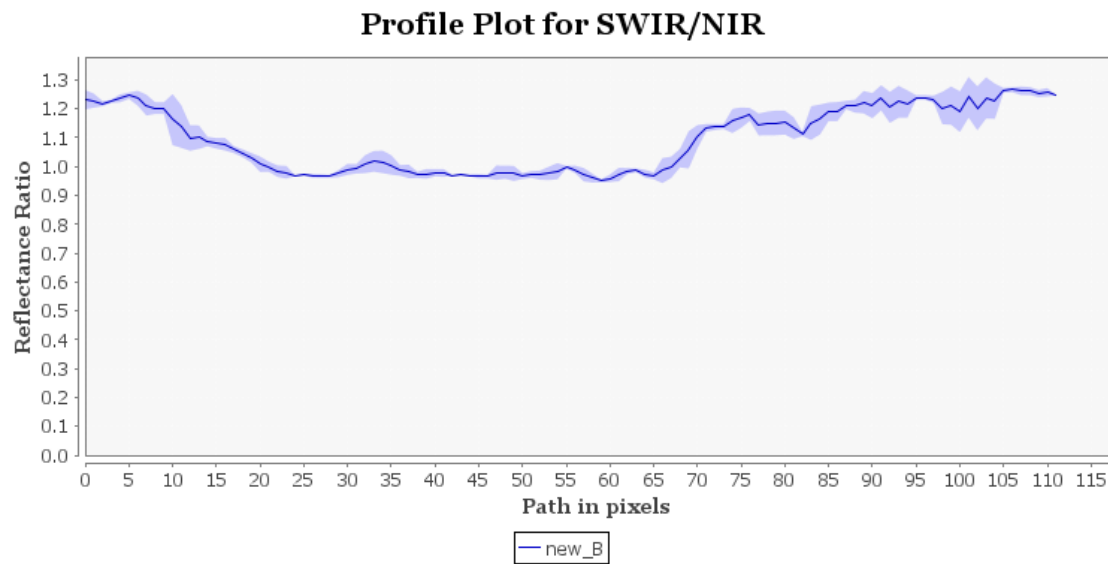


Figure 10: Transect Plot of Cloud Shadow

True Colour and False Colour Composite for Aug 06

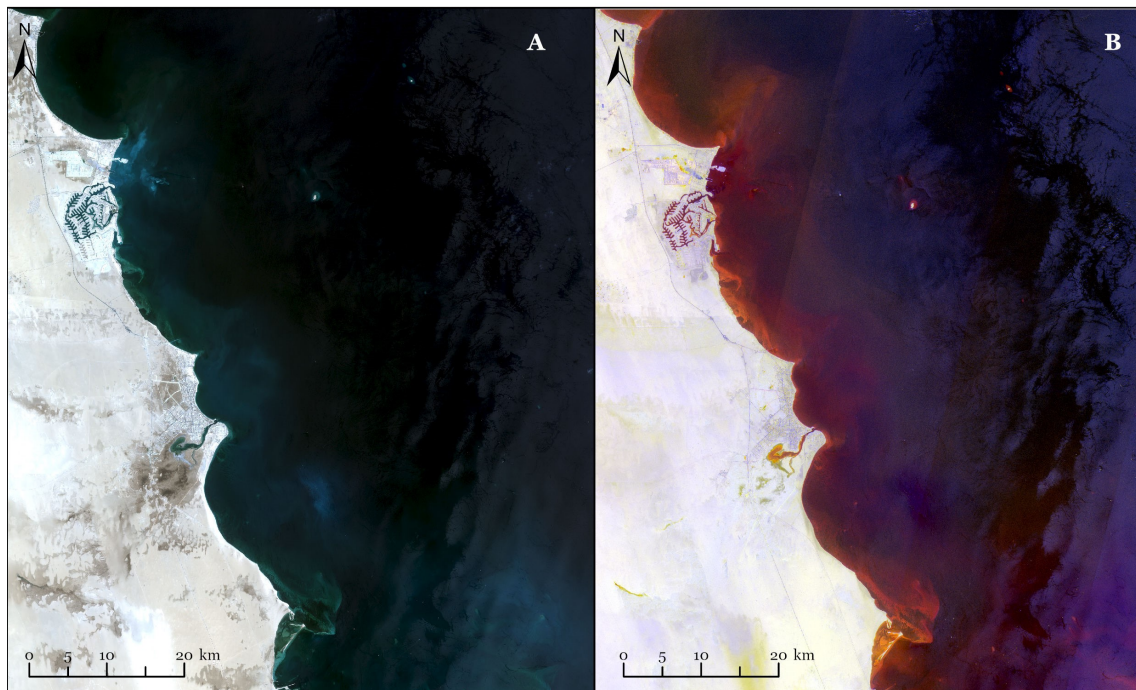


Figure 11: True colour and False Colour composites on August 6th

Classification Results overlaid FCC on Aug.11 2017

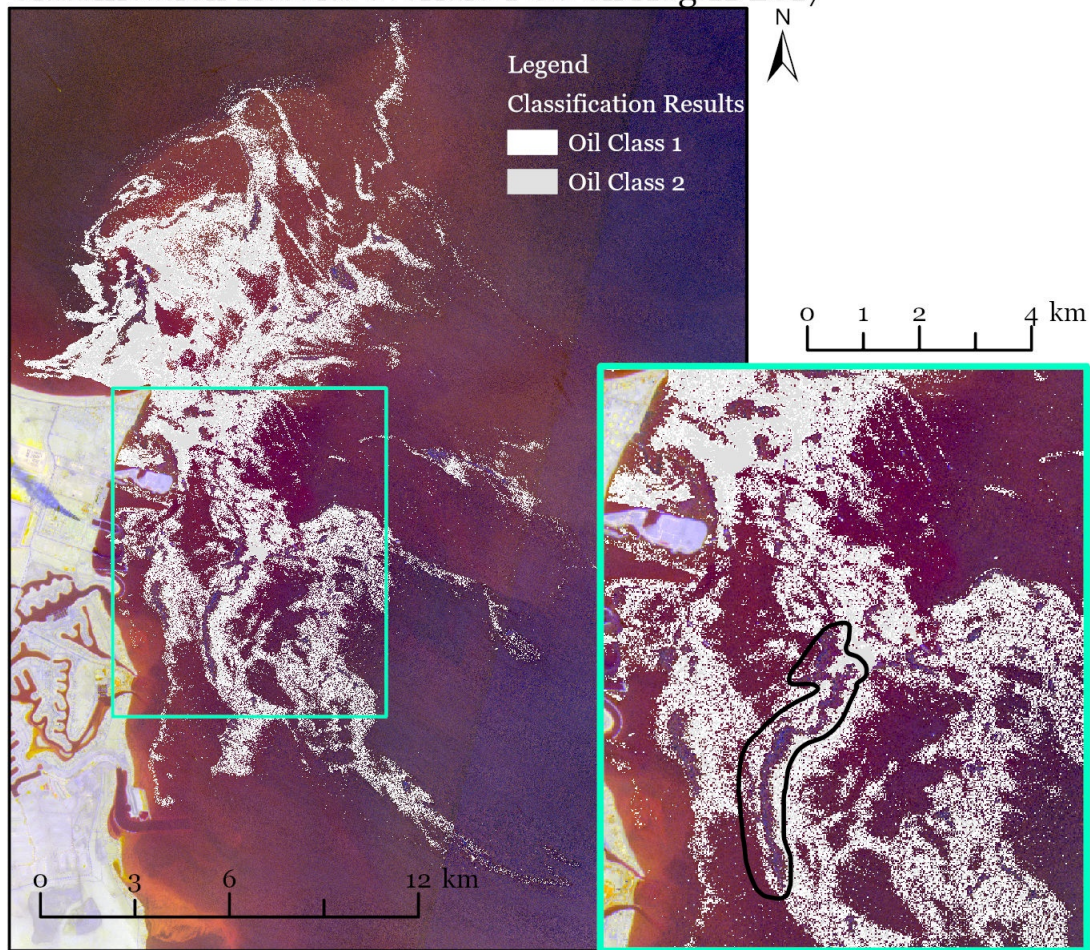


Figure 12: K-means classification Results from Aug 11

Classification Results overlaid FCC on Aug. 16 2017

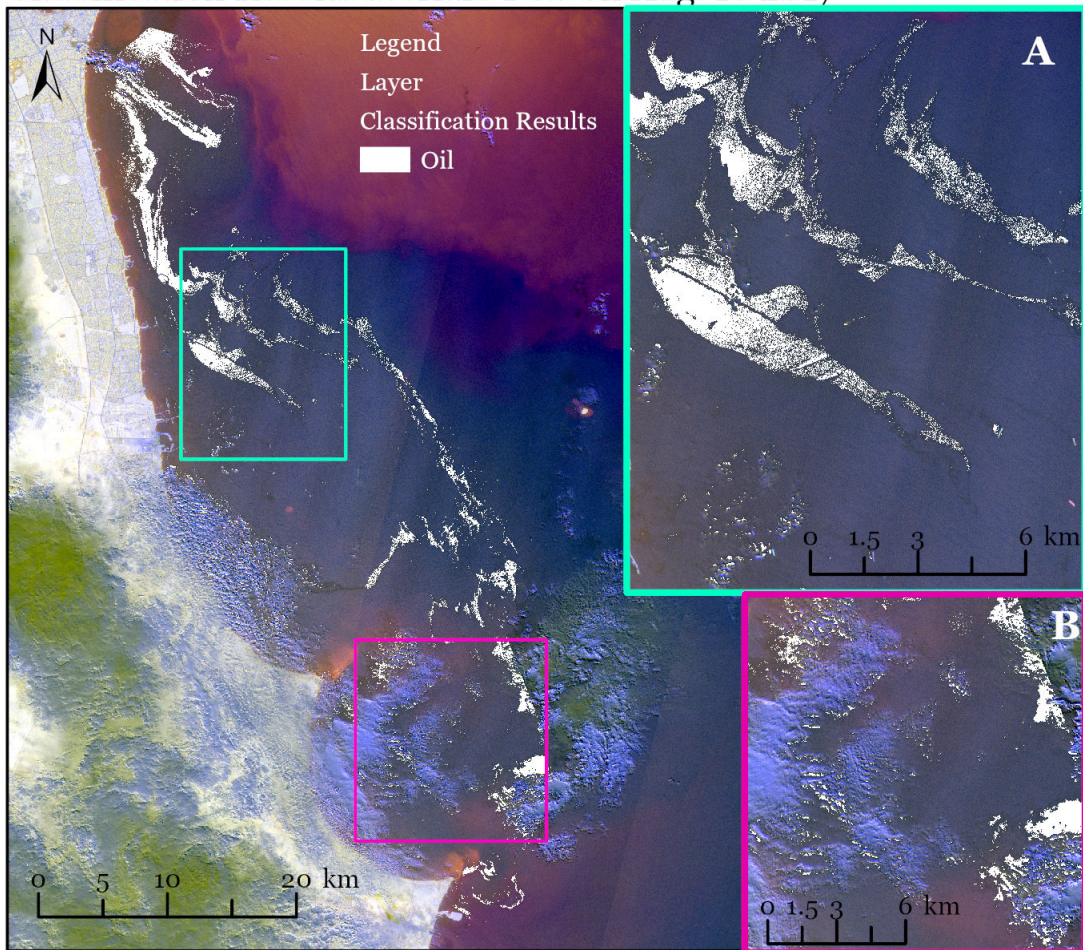


Figure 13: K-means classification Results from Aug 16

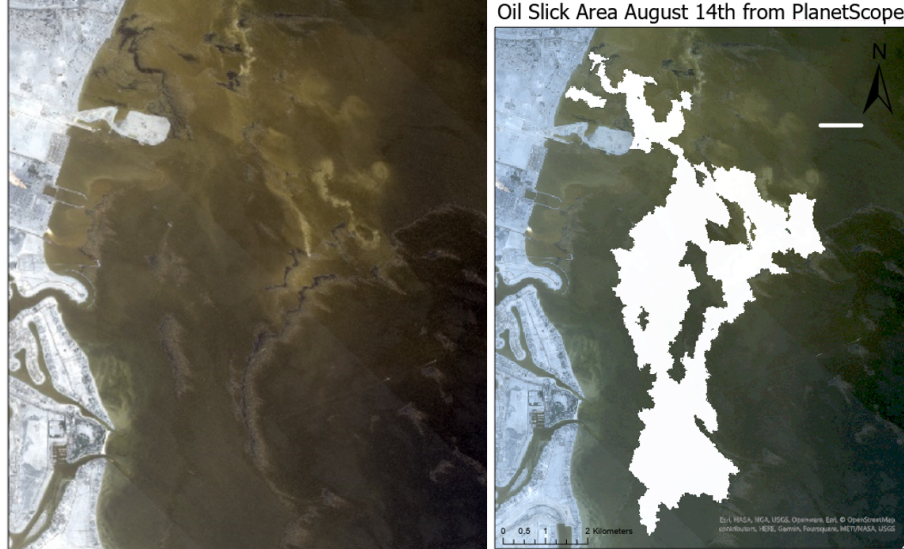


Figure 14: Comparison of Planetscope true colour images vs oil spill extracted by eCognition.

3.5 Classification Based on Combined Results

The results of each sensor were mapped together to analyze the overall path of the oil as shown in Figure 15. This also allows for the comparison between each date to check if the path, size, thickness, and location changed as expected, to help verify the results. The results show how the oil flowed into the coastal area, and then moved north along the coastline. This was as expected and matched the flow of currents recorded on these dates ([ear, 2023](#)). The change in size also matches what was anticipated, the change in size over time is shown in figure 16. From the 5th to the 10th the size increase, but the relative thickness decreases (damping ratio of 2.38 then 0.618) indicating that oil may be spreading out, but still the same in volume. On the 10th and 11th the size remains about the same. Although figure 16 shows a large decrease in size between Sentinel-1 to Sentinel-2 and Planet this is due to Sentinel-2 being better at detecting thin oil, and Planet at thick oil. Combined, with some overlap, the two sensors equate to roughly the same amount as detected by Sentinel-1 ($78+57 = 135$ vs 130). Moving to the 15th, and 16th the area and thickness (damping ratio now 0.34) have both decreased. This is anticipated as cleaning of the oil slick was reported by the 13th ([Jazeera, 2017](#)).

All dates between August 10th and 16th can thus confidently be classified as oil as they follow the expected currents, location, and size changes anticipated from the original

confirmed location on August 10th, across the results of all three sensors.

August 5th (dark red in Figure 15) is not classified with confidence. Although the change in size seems plausible, the currents do not match the expected movement, and Sentinel-2 imagery from August 6th does not identify oil. This is a source of uncertainty, further discussed in the discussion section.

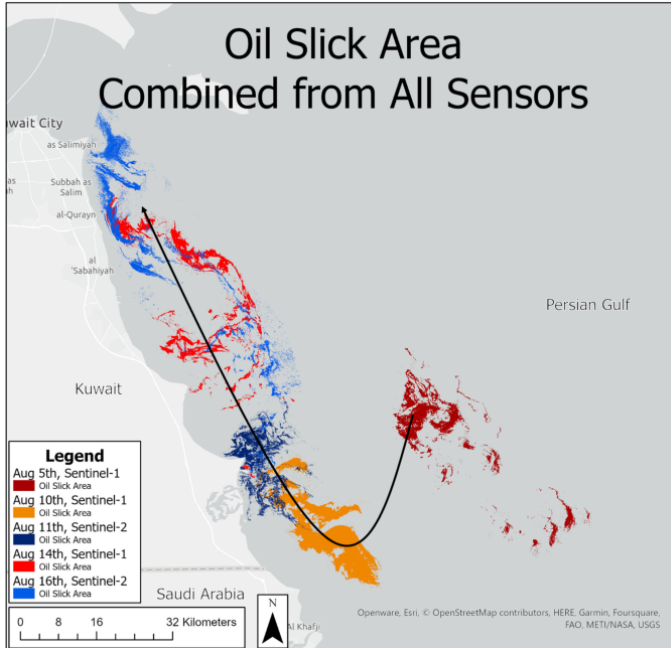


Figure 15: The tracked path that the oil slick followed as detected from all sensors combined.

4 Discussion

4.1 Planetscope Limitations

While PlanetLabs is still growing their constellations, there are currently still a lot of limitations when it comes to oil spill detection with Planetscope. One of the biggest drawbacks of Planet is the limited number of images that are available in marine areas. PlanetScope will gather data up to several kilometers from the coast of the ocean, but there are problems with accurate georeferencing due to the lack of accurate control points

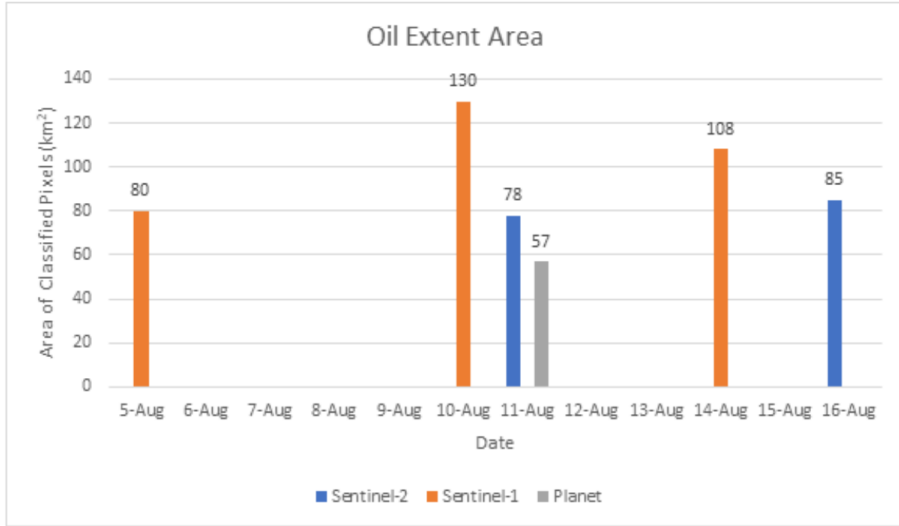


Figure 16: Total oil area measured over time by all sensors.

(Schaeffer et al., 2022). The accuracy of images off the shore ranges from 195 meters up to 1.4 kilometers whereas on land the accuracy only ranged from 1 meter to 2.72 meters (Schaeffer et al., 2022). With unreliable georeferencing, it can lead to inaccurate placing of the oil spill even if proper detection was done on the PlanetScope data. Moreover, PlanetScope does not acquire data beyond 15 kilometers from the shore, which leads to a limitation on locating oil spills that are happening further away from the coast (Schaeffer et al., 2022). This was one of the reasons why the study area of this paper had to be off the coast of the Persian Gulf. With PlanetScope data only going off 15 meters of the coast, it makes it impossible to use this satellite for oil spills in the middle of the Gulf. This is problematic since the most common oil spills come from ships transporting the oil or from rigs that are located further from the shore. Even though Plant only offers 15 kilometers off the coast generally, it is possible to request images to be taken in specific marine areas. However, this would take a lot of time to obtain data and for oil spills this is not a method that can be used after the oil spill already happened.

Another limitation is the low number of bands that PlanetScope has. The low number of bands make it very hard to find and detect oil spills since the most common wavelengths to detect oil in optical imagery are not there or is in the NIR band but not at the Planet NIR band. This takes away one of the strongest reasons to use optical satellites in oil spill management which is to determine false positives. Sentinel-2 does very well in utilizing its many bands to create false-colour composites that enhance the detected areas to visually

confirm whether or not the area is oil. With the limited amount of bands, it is hard to accurately detect oil on top of visually confirming oil slicks.

In order to overcome the limitations of the bands, the most common detection method that is paired with Planetscope imagery is neural networks and OBIA methods. These methods, however, only work best with imagery where the oil can be visibly seen before even using the detection methods. This is why for this study there was only 1 date that could be used during the 10 day time frame. Since PlanetLabs use optical satellites it is common that the imagery are often covered by clouds and with a small time frame of 10 days, it is common that a lot of the images can be at least partially blocked by clouds. Moreover, the oil needs to be visibly seen on that day which makes it even harder to locate the right images to use. On top of the difficult data collection process, many studies determined that a convoluted neural network with lots of accurate training data is needed to produce the best results. This leads to longer time needed for training the neural network and more complicated methods to get the same detection accuracy that SARS detection methods have now ([Park et al., 2019](#)).

4.2 Sentinel-1 Discussion

4.2.1 Uncertainties and Drawbacks

As mentioned in Methods, dark spots were classified based on existing criteria from other studies, with the addition of how the size, thickness, and location changed relative to known oil areas, and how it matched other available imagery without oil. This did seem to be effective as the resulting oil map does seem to follow a plausible path. But this method does come with one major drawback, to compare to known oil, it must first be known that at least one of the dark spots is oil. This was possible for the Kuwait oil spill as the results for oil area on August 10th, is confirmed as oil by a tutorial focusing on oil spill detection of the same image ([cop, 2017](#)). Without a known reference it would make things more difficult. When trying to initially find an oil slick to track, an oil spill off the coast of Lima, Peru was investigated. There, many of the dark spots seen in Sentinel-1 could be ruled as not oil since they were not seen in Sentinel-2 imagery. This demonstrates that the use of the two sensors together can classify dark spots as look-alikes even without a known reference. However, classifying a dark spot as oil because it is observed in both cannot be done with absolute certainty. It is still possible that there could be apparent oil in both Sentinel-1 and Sentinel-2 while being a look-alike. This is one large point of uncertainty.

Although increasing the factors that are considered when classifying oil vs look-alikes has increased the confidence of classifications, it is still important to note that there is

still not 100% certainty. It is still possible that some dark spots may have been classified incorrectly. The dark spot that contained the most uncertainty was August 5th. August 5th was a large source of uncertainty due to it being so far apart in dates from any other detected oil. Comparing from the 5th to the 10th (the next closest Sentinel-1 detected oil) the oil increased in area from 80,000 km² to 130,000 km², while the oil thickness decreased with damping ratios of 2.380 then 0.618. Even though there is a large change in area size, this would make sense if the thickness significantly decreased. This would mean that the oil is spreading out, so the same volume of oil may be represented by a larger area, with lower thickness. However, no news sources reported the presence of oil on August 5th and the initial report of oil was not until 5 days after. But with no confirmation of the source of the spill ([Jazeera, 2017](#)), the lack of news on August 5th could be either due to the oil not yet being spotted as it was offshore or due to the dark spot being a look-alike.

Sentinel-2 imagery from August 6th was analyzed to determine if the dark spot detected on August 5th is oil or a look-alike. The true colour imagery does not provide any useful information as all water is very dark right where the oil would be. The false colour composite shows a very large dark spot that encompasses the location of the dark spot detected on August 5th (Figure 11). It spans approximately 80 km from north to south and it appears it extends northward and southward. The dark area in Figure 11 appears to be too large for it to be all oil and does not seem to follow the trajectory of the oil spill. The values for the blue ratio are lower than the oil seen on August 11 and 16 suggesting it is not oil. If it's not oil, a possible explanation to the higher absorption and decreased reflection in the sea is The dark area has higher absorption and less light is being reflected which can be due to changes in surface currents, or a lack of wind that are cause the surface of the water to become smoother (CITE). Unfortunately, without in-situ data this cannot be confirmed.

August 6th highlights the drawbacks of relying on optical imagery to validate SAR look-alikes. There is not enough research that shows how other features on the water would look like using the band ratios. And not all dark areas in false colour composites would be oil. Because of this, the dark spots detected by SAR sensors cannot be conclusively visually determined. Another addition that could have been made or could be made in future research would be more testing of dark spot classification methods using SAR. From the literature review (and as mentioned earlier), many of the dark spot detection studies cited back to a 1999 study which stated subjective methods for classifying dark spots; spots are likely to be oil if they are near a platform or ship, if they have a strong contrast to the open water, etc. ([Solberg et al., 1999](#)). However, other classification methods do exist that seem to be less explored. For example, one study by [Liu et al. \(2010\)](#) examines the use of fuzzy logic algorithms to classify dark spots. This process involved training a fuzzy model based

on imagery including 120 oil slicks, and 80 look-alikes. The fuzzy model produces many if-then statements such as: “if x is small, and y is large, and z is small . . . then the probability of oil slick is high” which can be used to classify future oil slicks. The variables (x , y , z ...) represent factors about the dark spot such as complexity or form factor (details about the shape of the dark spot), backscatter levels, smoothness, among others. This study shows decent accuracies of around 80%, but only for a small sample size, which indicates strong potential for the method but not enough proof. Another study by [Aghaei et al. \(2022\)](#) uses SVM (a machine learning method) to produce initial contours to run level-set segmentation (a supervised classification method based on topology) to classify dark spots. Although the study shows results are claimed to be accurate it does not compare to any expected results or give numerical accuracy. Overall, from the literature, no one method has been agreed upon as being effective enough to become the standard for dark spot classification. This is an area for future research, as the methods show the potential that if improved upon would greatly improve the results of any system for tracking oil slicks.

4.2.2 SNAP OS Detection

Also available for Sentinel-1 data was the oil spill detection tool within SNAP ([cop, 2017](#)). This was tested and compared to the results from k-means. Both showed strong results but also showed slight inaccuracy. While the k-means seemed to misclassify some open water as oil, the oil spill detection tool seemed to do the opposite, by underestimating the oil area. The extent drawn seemed to be within the dark spot, with some areas in the dark spot being identified as water. Figure 17 shows the misclassification in both methods, the right shows how the SNAP tool has drawn a mask over the SAR image, but still many black spots stick out beyond the mask. Unfortunately, without a true extent, an accuracy matrix could not be created to determine the percentage of pixels correctly classified. However, from subjective accuracy assessment, it appeared that both methods provided similar accuracy, just with the difference being overestimation versus underestimation. The oil spill detection algorithm also provided the benefit of producing additional vector layer results, and masks while k-means only returned a raster. However, for the purpose of this study, a raster was adequate. Overall k-means was used due to a much faster runtime, but either method would've provided sufficient results.

4.3 Sentinel-2 Band Ratios

The different types of oil seen in Figure 5 can be explained by oil’s spectral properties. Floating black oil is the thickest and as its name suggests it is black. Consequently, it has

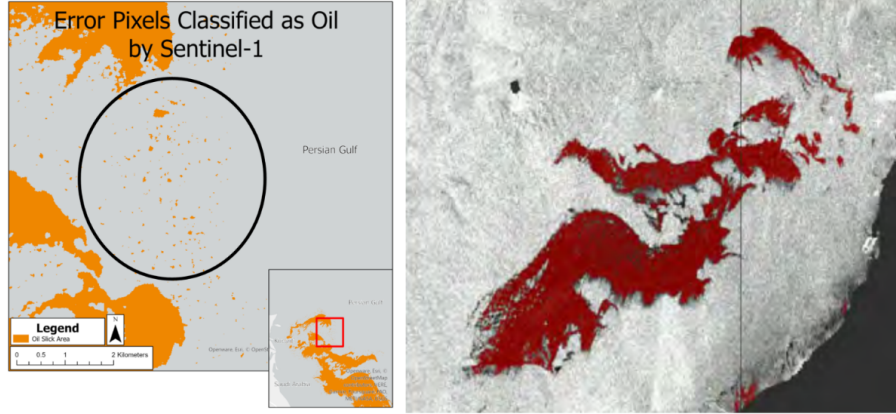


Figure 17: Left image shows results from k-means which classifies extra water as oil, Right image shows results from SNAP’s OS Detection tool tutorial [cop \(2017\)](#), where some oil is not detected by the tool, and sticks out beyond the mask.

low brightness because of the strong absorption, low reflection of light ([Lu et al., 2013](#)). For oil slicks, as oil thickness increases the spectral reflectance decreases as more light gets absorbed which differs from thin oil slicks which have a higher reflectance than the background seawater. This results in different colours of sheens, rainbow sheen, metallic sheen etc. The Bon Agreement Oil Appearance Code contains a visible guide of different oil colours and their approximate thickness ([Ivanov and Gerivani, 2021a](#))

The background seawater needs to have a high stable response so that the lowered reflectance of oil slicks can be detected in a true colour image ([Lu et al., 2013](#)). In the Sentinel-2 images the seawater response is dark with low reflectance so the difference in spectral response of water and oil in the visible range is not enough to be seen on Aug 16 as no oil slicks can be seen in the true colour composite. Therefore, band ratios are truly necessary to maximize the contrast and visualize the near-infrared and shortwave infrared ranges of the EM spectrum. The band combinations that previous studies have used ([Gafoor and Al Shehhi, 2022; Rajendran et al., 2021a,b; Abou Samra and Ali, 2022](#)) did not yield the largest contrast between oil and the water. The red ratio was combined with the green and blue ratio of the other combination produced by ([Rajendran et al., 2021a](#)). The ratios are calculated by “summing up the bands representing the shoulders of absorption features in the numerator and the band located near the absorption feature in the denominator” ([Rajendran et al., 2021a](#)), meaning that the reflectance of B8 and B2 in ratios $(B11+B12)/B8$ and $(B3+B4)/B2$, are what is being exaggerated. Since the study area does not have large presence of algae or vegetation the ratios $(6 + 7)/5$ and $(5$

$(B1+6)/7$ were not used as they are used to show the vegetation related information (Gafoor and Al Shehhi, 2022). The clearest oil detection ratio from Rajendran et al. (2021a), was $(B3+B4)/B2$; this study found $(B11+B12)/B8$ to show the most contrast (Figure 8). Because of a lack of in-situ data and no spectrometer, an in-depth analysis of the spectra of this particular oil spill was not done. Future research can provide evidence as to why ratio $(B11+B12)/B8$ has the most contrast between the water and oil.

While this approach and the band combinations worked to detect oil that had similar responses to water in the visible range, the band ratios did not do well at displaying the black oil visible on the true colour images. Instead, they appear as the surrounding water. This is because the oil had similar reflectance in bands 8, 11 and 12. Consequently, the amount of oil was underestimated after the classification. In this study, a ratio that can distinguish between black oil and the rest of the water would be beneficial. However, the similar reflectance response between water and the black oil impedes its separation. An image with a higher contrast between water and black oil will be favourable, however if that is not possible, including a hyper-spectral sensor would provide more bands that can help distinguish the water's response and the black oil (Kang et al., 2022; Lu et al., 2013) but a new sensor comes with more limitations like the narrow swath width and the data noise and low data quality (Yang et al., 2020).

Conversely, oil was overestimated if there are clouds since cloud shadows were misclassified as oil. As seen in Figure 10 and 9, the ratio value is similar enough that the K-means classifier was not able to tell them apart. So, a cloud free image is imperative for these ratios to work. Another limitation is that the band ratio approach only works if there is prior knowledge of the oil. Without prior knowledge dark areas can be confused with other substances. Research is limited as to what substances or environmental condition can cause this confusion. The image from August 6th is a perfect example showing a dark area that may or may not be oil (More information in section 4.2.1). So, as of now, the band ratios cannot be used in automatic detection.

The band combination and ratios appear to be very dependent on the location, and environmental conditions so more research in this area will be needed if this technique will be used for automatic detection. Future research on the band ratios to test its robustness across various sites with differing environmental and climatic conditions would be beneficial. This study experimented with the ratios to produce the optimal combination that maximized visual distinction of oil however it is not known if every site would require a different combination or even different ratios. A study that will test if such a combination exists would be beneficial to save time and expand this technique in oil detection in the literature and practical applications. Additionally, the creation of a standard legend of features' colours with a band combination would also be beneficial to the expansion of

this technique. For example, suspended sediment appears yellow, clouds green etc. Also researching, with in-situ data measured by spectrometers, the response of common look-alikes and adding this to the legend will be ideal. Besides all the limitations of the band ratios and combinations, they have a lot of potential for Sentinel-2 oil spill detection especially because it visualizes oil slicks when the true colour imagery cannot. So, more research is needed to reduce or work around the limitations.

4.4 K-Means Clustering

K-means clustering was used to identify the oil areas after preprocessing of both Sentinel-1 and Sentinel-2 imagery. However, there are other methods that could have achieved similar results such as EM Cluster Analysis, or supervised classification methods. Due to time constraints on the project, only k-means was used, as it yielded strong results. In future research, it is possible that these other methods could be compared to k-means for the purpose of dark-spot detection and could possibly yield better results. One study comparing k-means and EM Clustering (unrelated to oil detection) found the two to have similar results, but also found that both were sensitive to noise in the data [Abbas \(2008\)](#). The high speckle in Sentinel-1 data, even after preprocessing, may imply that other clustering methods that were not explored (hierarchical clustering or self-organizing maps) may be more effective.

The number of classes by k-means could have also been modified to possibly increase results. The classes were modified and k-means was run on a few number of classes: 2, 4, 16, 32. The desired outcome of this was that error clusters, such as those shown in Figure 4, would be classified separately from oil with more classes, and could be marked as water. However, this was not the case and even with more classes, the clusters were still mixed with oil classes. This could be due to too much similarity in backscatter coefficients between these pixels. Or, possibly more experimentation with the number of classes could have resolved this issue. Overall, 4 was selected for the number of classes due to sufficient results, and being the simplest to reclassify to oil and water.

Sentinel-2-Classification

For Sentinel-2 imagery the quality of the k-means classification depended on the quality of the false colour composite, the higher the contrast between water and oil, the better the classification. While a formal quantitative accuracy assessment was not performed due to a lack of ground truth data, visually, the classification results are compared. August 16th mostly had false negatives which underestimates the amount of oil. The classification results for August 11th are poorer with false negatives and false positives because of the low

contrast of the oil and the water surrounding it. However, the quantity of oil calculated for August 16th, is larger than the amount of oil calculated on August 11. This is not expected since it is assumed that the quantity of oil would decrease as time goes on because of oil weathering processes ([Garcia-Pineda et al., 2013](#); [Mishra and Kumar, 2015](#)) and cleaning efforts by the Kuwait administration ([Calcuttawala, 2017](#)) There are multiple explanations why this is the case. The oil spill in the August 16 image is spread out over a larger area (approx. 800 km) as two Sentinel-2 images needed to be mosaicked. So, more pixels contributed to the oil class creating a larger area estimate. Plus, a larger area, means that more water pixels were misclassified as oil. Lastly, the area estimate for August 11 does not include the visible black oil, and the classified oil slicks are patchy with missing pixels which decreases the area estimation which increases the difference between the area estimates of both dates. K-means Clustering is not the best classification method for the Sentinel-2 data because the location of oil slicks is not as clear as it is with Sentinel-1 data. Additionally, because it is pixel-based classification, the algorithm individually classifies each pixel which create the noisy results plagued with false negatives because the pixel values within the oil slicks are not as uniform and are patchy. This suggests that a pixel-based approach for optical imagery is not adequate and an image segmentation and object based image analysis may improve performance as it takes into consideration the neighbourhood around the pixels which can indicate the regions and better capture the shape of the oil slicks ([Karantzalos and Argialas, 2008](#); [Mohammadi et al., 2021](#)) . Object-based Image analysis is the preferred classification method for oil slicks ([Karantzalos and Argialas, 2008](#); [Al-Ruzouq et al., 2020](#)).

4.5 Ideal Oil Spill Multi-Sensor System Specifications

The following is an idealized sensor system that would provide maximum accuracy and confidence, based on the overall results and review of literature. This demonstrates how the benefits of using multiple sensors could be maximized. The possibility of more sensor availability is also included in this section. For example, the ideal sensor may have access to non-public sensors such as TerraSAR-X. However, this may only be possible if the system were being designed by a company such as NASA that has the resources and connections to acquire this data.

Dark Spot Detection

SAR data was found to be the most effective for dark spot detection, both from the results and from the literature review. Sentinel-1 provided strong results but lacked in having a slow repeat time. Other SAR satellites would be used to fill in the gaps because

of this, such as RadarSAT-2, and TerraSAR-X among others. All of these have low repeat times but together could hopefully fill as many gaps as possible. All SAR sensors could undergo the same preprocessing as described in the methods section. K-means, SNAP's OS detection tool, among other methods could be used as the dark spot detection algorithm. Strong accuracy was shown from all methods, with the key being SAR imagery, as it has the most distinct contrast between oil and water.

Secondly, Sentinel-2 can be used to fill gaps in days that are not covered by SAR imagery. Even though there was some difficulty distinguishing between thick oil and water with Sentinel-2, it was still strong at identifying the general shape of the thin oil. More research can be done to find a band combination that can visualize the dark oil and reduce the limitation. This is beneficial for keeping track of where the oil goes for periods where there are large gaps between available SAR images.

Classification

Due to the uncertainty of any one classification method, the ideal system will combine multiple sources to maximize confidence in classification. Firstly, Sentinel-2 can be used to check if the oil detection matches with the SAR dark spot detection. This was strong in classifying look-alikes but was not conclusive in classifying oil (as discussed earlier). Secondly, SAR-based classification can be applied. Both subjective (contrast, homogeneity of background, etc) or automated (fuzzy model). Thirdly, the context of size, thickness, and location compared to other known oil areas can be analyzed, to see if the path of the oil seems realistic. Together if all three methods suggest oil, it can be concluded with high confidence that a dark spot is oil. Lastly, but less prominent to remote sensing, news or other sources of available information about the area should be considered by the system operator. This is the ultimate way to be confident in classification. This is not dissimilar from other studies that also mention confirming dark spots by plane ([Brekke and Solberg, 2005](#)).

Thickness

MODIS data was found to have too low of a resolution to be of use for the Kuwait oil slick, or tested in this study. However, based on existing literature, the ideal sensor would be able to estimate the oil thickness when tracking a larger spill that can be seen by MODIS. Thickness can be calculated based on the brightness temperature difference ([Lu et al., 2016](#)). This is calculated using a relationship identified between the brightness temperature difference and the depth of oil, shown below. The brightness temperature difference (BTD) can be found by taking the average brightness temperature of oil (based on dark spot detection area), the average brightness temperature of the surrounding water, and taking the difference.

$$\text{EOT (thickness in mm)} = [1.29e^{(0.16*\text{BTD})} - 1.29] \left(\frac{12.2}{\text{ocean surface air temp}} \right)$$

Drawbacks

Overall, this system would provide maximum accuracy and confidence in classifications and detection. The major drawback to this system would be that by combining so many sensors it would require much more work to gather the datasets and apply the methods. Especially with the use of non-public sensor data, such as TerraSAR-X, where access to data must be requested. Because of this, depending on your desired results, this tradeoff may not be worth it. In a situation where the location of an oil spill is known and an estimate of the total area covered is desired, the combination of sensors and extra time to collect/process more data would be unnecessary as Sentinel-1 alone could do a sufficient job.

5 Conclusion

In conclusion, the oil slick in Kuwait was successfully detected and tracked by the multi-sensor system. The major benefits of a multi-sensor system were that the confidence in the classification of dark spots as oil versus look-alike was increased by comparing SAR dark spots, to where oil was identified in Sentinel-2 and Planet imagery. Without these additional sensors, dark spot classification was extremely difficult based only on SAR imagery. Secondly, the use of different sensors allowed for an increased repeat time, gap-filling the dates that were available had Sentinel-1 been used independently. Thirdly, Planet and Sentinel-2 complimented each other well as Sentinel-2 was better at detecting thin oil while Planet was better at detecting thick oil. However, the use of three sensors also contains limitations and uncertainties. The available area for tracking is limited, due to Planet data only being available near coastlines. Also, even with the use of all three, some dark spots still cannot be classified with absolute certainty. Overall, the use of three sensors together still provided a more confident classification than if any one sensor had been used individually.

The lack of in-situ data was the largest challenge faced in this study. Without in-situ data, it was very difficult to calculate the accuracy of the results or determine with 100% accuracy if some dark spots were oil. Future research may benefit from focusing on oil slicks that have already been explored by previous studies. This would allow for some known oil and look-alike examples, and a reference to compare how results have improved or decreased in comparison to the original study.

Some future areas of study identified were further research into dark spot classification using SAR data, the use of other object-based image analysis methods for oil detection in Sentinel-2 data, and the creation of an oil spill and look-alike database, a current gap which would greatly assist all future research on oil spill detection.

References

- Sentinel-2 msi - technical guide - sentinel online. URL <https://sentinel.esa.int/web/sentinel/technical-guides/sentinel-2-msi>.
- Monthly sea level pressure. URL https://iri.ldeo.columbia.edu/maproom/Global_Atmospheric_Circulation/Sea_Level_Pres.html?bbox=bb%3A9.01%3A2.32%3A92.01%3A47.50%3Abb&T=Aug%202017.
- Training kit - ocea03. Website, 2017. URL https://eo4society.esa.int/wp-content/uploads/2022/01/OCEA03_OilSpill_Kuwait.pdf.
- What is synthetic aperture radar?, Apr 2020. URL <https://www.earthdata.nasa.gov/learn/backgrounders/what-is-sar>.
- Earth, 2023. URL <https://earth.nullschool.net/>.
- Modis web, n.d. URL <https://modis.gsfc.nasa.gov/about/>.
- Sustainable development goals, n.d. URL <https://sdgs.un.org/goals/goal14>.
- Planet monitoring - satellite imagery and monitoring, n.d. URL <https://www.planet.com/products/monitoring/>.
- O. A. Abbas. Comparisons between data clustering algorithms. *International Arab Journal of Information Technology (IAJIT)*, 5(3), 2008.
- R. M. Abou Samra and R. R. Ali. Monitoring of oil spill in the offshore zone of the nile delta using sentinel data. 179:113718, 2022. ISSN 0025-326X. doi: 10.1016/j.marpolbul.2022.113718. URL <https://www.sciencedirect.com/science/article/pii/S0025326X22004003>.
- B. Adamu, K. Tansey, and B. Ogunjuwa. Remote sensing for detection and monitoring of vegetation affected by oil spills. 39(11):3628–3645. ISSN 0143-1161. doi: 10.1080/01431161.2018.1448483. URL <https://doi.org/10.1080/01431161.2018.1448483>. Publisher: Taylor & Francis .eprint: <https://doi.org/10.1080/01431161.2018.1448483>.
- E. Agamy. Sub chronic exposure to crude oil, dispersed oil and dispersant induces histopathological alterations in the gills of the juvenile rabbit fish (*siganus canaliculatus*). 92:180–190, 2013. ISSN 0147-6513. doi: 10.1016/j.ecoenv.2013.03.027. URL <https://www.sciencedirect.com/science/article/pii/S0147651313001152>.

- N. Aghaei, G. Akbarizadeh, and A. Kosarian. Greywolfslsm: An accurate oil spill detection method based on level set method from synthetic aperture radar imagery. *European Journal of Remote Sensing*, 55(1):181–198, 2022.
- R. Al-Ruzouq, M. B. A. Gibril, A. Shanableh, A. Kais, O. Hamed, S. Al-Mansoori, and M. A. Khalil. Sensors, features, and machine learning for oil spill detection and monitoring: A review. *Remote Sensing*, 12(20):3338, 2020.
- W. Alpers, B. Holt, and K. Zeng. Oil spill detection by imaging radars: Challenges and pitfalls. 201:133–147, 2017. ISSN 0034-4257. doi: 10.1016/j.rse.2017.09.002. URL <https://www.sciencedirect.com/science/article/pii/S0034425717304145>.
- S. Angelliaume, X. Ceamanos, F. Viallefont-Robinet, R. Baqué, P. Déliot, and V. Miegebielle. Hyperspectral and radar airborne imagery over controlled release of oil at sea. 17(8):1772, 2017. ISSN 1424-8220. doi: 10.3390/s17081772. URL <https://www.mdpi.com/1424-8220/17/8/1772>. Number: 8 Publisher: Multidisciplinary Digital Publishing Institute.
- A. Ben-Hasan and M. Daliri. Arabian/persian gulf artisanal fisheries: magnitude, threats, and opportunities. 2022. ISSN 1573-5184. doi: 10.1007/s11160-022-09737-4. URL <https://doi.org/10.1007/s11160-022-09737-4>.
- C. Brekke and A. H. Solberg. Oil spill detection by satellite remote sensing. *Remote Sensing of Environment*, 95(1):1–13, 2005. ISSN 0034-4257. doi: <https://doi.org/10.1016/j.rse.2004.11.015>. URL <https://www.sciencedirect.com/science/article/pii/S0034425704003724>.
- Z. Calcuttawala. Second oil spill reported in kuwait’s ras al-zour waters, Aug 2017. URL <https://oilprice.com/Latest-Energy-News/World-News/Second-Oil-Spill-Reported-in-Kuwaits-Ras-Al-Zour-Waters.html>.
- G. Capizzi, G. Lo Sciuto, M. Woźniak, and R. Damaševicius. A clustering based system for automated oil spill detection by satellite remote sensing. In L. Rutkowski, M. Korytkowski, R. Scherer, R. Tadeusiewicz, L. A. Zadeh, and J. M. Zurada, editors, *Artificial Intelligence and Soft Computing*, pages 613–623, Cham, 2016. Springer International Publishing. ISBN 978-3-319-39384-1.
- G. Caporusso, C. Gallo, and E. Tarantino. Change detection analysis using sentinel-1 satellite data with snap and gee regarding oil spill in venezuela. In *Computational Science and Its Applications–ICCSA 2022 Workshops: Malaga, Spain, July 4–7, 2022, Proceedings, Part III*, pages 387–404. Springer, 2022.

- Y. Dong, Y. Liu, C. Hu, I. R. MacDonald, and Y. Lu. Chronic oiling in global oceans. 376(6599):1300–1304, 2022. doi: 10.1126/science.abm5940. URL <https://www.science.org/doi/10.1126/science.abm5940>. Publisher: American Association for the Advancement of Science.
- M. Espeseth, H. Isaksen, and K.-F. Dagestad. Initiating oil spill drift model with thickness variations. In *proc. INTERSPILL*, volume 59, pages 129–135, 2022.
- N. Evtushenko, A. Ivanov, and V. Evtushenko. Oil pollution in the persian gulf: Satellite-monitoring results in 2017. In H. M. El-Askary, S. Lee, E. Heggy, and B. Pradhan, editors, *Advances in Remote Sensing and Geo Informatics Applications*, Advances in Science, Technology & Innovation, pages 343–347. Springer International Publishing, 2019. ISBN 978-3-030-01440-7. doi: 10.1007/978-3-030-01440-7_76.
- F. A. Gafoor and M. R. Al Shehhi. Oil spill detection and mapping using sentinel-1 and sentinel-2 in the arabian gulf coastal waters. In *IGARSS 2022 - 2022 IEEE International Geoscience and Remote Sensing Symposium*, pages 6745–6748, 2022. doi: 10.1109/IGARSS46834.2022.9883723. ISSN: 2153-7003.
- O. Garcia-Pineda, I. MacDonald, C. Hu, J. Svejkovsky, M. Hess, D. Dukhovskoy, and S. Morey. Detection of floating oil anomalies from the deepwater horizon oil spill with synthetic aperture radar. *Oceanography (Washington, D.C.)*, 26(2):124–137, 2013. ISSN 1042-8275.
- E. C. Government of Canada. Select ozone maps from archive. URL <https://exp-studies.tor.ec.gc.ca/cgi-bin/clf2/selectMap?lang=e&clf=2&printerversion=false&printfullpage=false&accessible=off&type1=du&day1=11&month1=08&year1=2017&howmany1=1&interval1=1&intervalunit1=d&hem1=g&type2=du&day2=16&month2=09&year2=2017&howmany2=1&interval2=1&intervalunit2=d&hem2=g&mapsize=100>.
- Y. Gunnell and A. Krishnamurthy. Past and Present Status of Runoff Harvesting Systems in Dryland Peninsular India: A Critical Review. *AMBIO: A Journal of the Human Environment*, 32(4):320–324, 2009. ISSN 0044-7447. doi: 10.1579/0044-7447-32.4.320.
- C. Hu, Y. Lu, S. Sun, and Y. Liu. Optical remote sensing of oil spills in the ocean: What is really possible? 2021:2021/9141902, 2021. ISSN 2694-1589. doi: 10.34133/2021/9141902. URL <https://spj.science.org/doi/10.34133/2021/9141902>.
- A. Y. Ivanov and H. Gerivani. Oil leaking and seeping site in the persian gulf detected and studied by satellite observations. 39(12):1481–1496, 2021a.

ISSN 1064-119X. doi: 10.1080/1064119X.2020.1853286. URL <https://doi.org/10.1080/1064119X.2020.1853286>. Publisher: Taylor & Francis eprint: <https://doi.org/10.1080/1064119X.2020.1853286>.

- A. Y. Ivanov and H. Gerivani. Oil leaking and seeping site in the persian gulf detected and studied by satellite observations. 39(12):1481–1496, 2021b. ISSN 1064-119X. doi: 10.1080/1064119X.2020.1853286. URL <https://doi.org/10.1080/1064119X.2020.1853286>. Publisher: Taylor & Francis eprint: <https://doi.org/10.1080/1064119X.2020.1853286>.
- A. Jazeera. Emergency teams battle to contain oil spill off kuwait. Website, 2017. URL <https://www.aljazeera.com/economy/2017/8/13/emergency-teams-battle-to-contain-oil-spill-off-kuwait>.
- M. Jefferson. A crude future? covid-19s challenges for oil demand, supply and prices. *Energy Research Social Science*, 68:101669, 2020. ISSN 2214-6296. doi: <https://doi.org/10.1016/j.erss.2020.101669>. URL <https://www.sciencedirect.com/science/article/pii/S2214629620302449>.
- J. Jiao, Y. Lu, C. Hu, J. Shi, S. Sun, and Y. Liu. Quantifying ocean surface oil thickness using thermal remote sensing. *Remote Sensing of Environment*, 261:112513, 2021. ISSN 0034-4257. doi: <https://doi.org/10.1016/j.rse.2021.112513>. URL <https://www.sciencedirect.com/science/article/pii/S0034425721002339>.
- X. Kang, Z. Wang, P. Duan, and X. Wei. The potential of hyperspectral image classification for oil spill mapping. 60:1–15, 2022. ISSN 1558-0644. doi: 10.1109/TGRS.2022.3205966. Conference Name: IEEE Transactions on Geoscience and Remote Sensing.
- K. Karantzalos and D. Argialas. Automatic detection and tracking of oil spills in SAR imagery with level set segmentation. 29(21):6281–6296, 2008. ISSN 0143-1161. doi: 10.1080/01431160802175488. URL https://journals.scholarsportal.info/details/01431161/v29i0021/6281_adatoosiwlss.xml. Publisher: Taylor & Francis.
- P. Kolokoussis and V. Karathanassi. Oil spill detection and mapping using sentinel 2 imagery. 6(1):4. ISSN 2077-1312. doi: 10.3390/jmse6010004. URL <https://www.mdpi.com/2077-1312/6/1/4>. Number: 1 Publisher: Multidisciplinary Digital Publishing Institute.
- K. Kvenvolden and C. Cooper. Natural seepage of crude oil into the marine environment. 23:140–146, 2003. doi: 10.1007/s00367-003-0135-0.

- D. Latini, F. Del Frate, and C. E. Jones. Multi-frequency and polarimetric quantitative analysis of the gulf of mexico oil spill event comparing different SAR systems. 183:26–42. ISSN 0034-4257. doi: 10.1016/j.rse.2016.05.014. URL <https://www.sciencedirect.com/science/article/pii/S0034425716302152>.
- J. S. Lee, L. Jurkevich, P. Dewaele, P. Wambacq, and A. Oosterlinck. Speckle filtering of synthetic aperture radar images: A review. *Remote Sensing Reviews*, 8(4): 313–340, 2009. doi: 10.1080/02757259409532206. URL <https://doi.org/10.1080/02757259409532206>.
- I. Leifer, W. J. Lehr, D. Simecek-Beatty, E. Bradley, R. Clark, P. Dennison, Y. Hu, S. Matheson, C. E. Jones, B. Holt, M. Reif, D. A. Roberts, J. Svejkovsky, G. Swayze, and J. Wozencraft. State of the art satellite and airborne marine oil spill remote sensing: Application to the BP deepwater horizon oil spill. 124:185–209, 2012. ISSN 0034-4257. doi: 10.1016/j.rse.2012.03.024. URL <https://www.sciencedirect.com/science/article/pii/S0034425712001563>.
- P. Liu, C. Zhao, X. Li, M. He, and W. Pichel. Identification of ocean oil spills in sar imagery based on fuzzy logic algorithm. *International Journal of Remote Sensing*, 31 (17-18):4819–4833, 2010.
- Y. Lu, X. Li, Q. Tian, G. Zheng, S. Sun, Y. Liu, and Q. Yang. Progress in marine oil spill optical remote sensing: Detected targets, spectral response characteristics, and theories. 36(3):334–346, 2013. ISSN 0149-0419. doi: 10.1080/01490419.2013.793633. URL <https://doi.org/10.1080/01490419.2013.793633>. Publisher: Taylor & Francis eprint: <https://doi.org/10.1080/01490419.2013.793633>.
- Y. Lu, W. Zhan, and C. Hu. Detecting and quantifying oil slick thickness by thermal remote sensing: A ground-based experiment. *Remote Sensing of Environment*, 181: 207–217, 2016. ISSN 0034-4257. doi: <https://doi.org/10.1016/j.rse.2016.04.007>. URL <https://www.sciencedirect.com/science/article/pii/S0034425716301559>.
- F. Löw, K. Stieglitz, and O. Diemar. Terrestrial oil spill mapping using satellite earth observation and machine learning: A case study in south sudan. 298:113424. ISSN 0301-4797. doi: 10.1016/j.jenvman.2021.113424. URL <https://www.sciencedirect.com/science/article/pii/S0301479721014869>.
- F. Mialhe, Y. Gunnell, and C. Mering. Synoptic assessment of water resource variability in reservoirs by remote sensing : General approach and application to the runoff

- harvesting systems of south India Franc. *Water Resour. Res.*, 44:1–14, 2008. doi: 10.1029/2007WR006065.
- B. Minchew, C. E. Jones, and B. Holt. Polarimetric analysis of backscatter from the deepwater horizon oil spill using l-band synthetic aperture radar. *IEEE transactions on geoscience and remote sensing*, 50(10):3812–3830, 2012. ISSN 0196-2892.
- A. K. Mishra and G. S. Kumar. Weathering of oil spill: Modeling and analysis. 4:435–442, 2015. ISSN 2214-241X. doi: 10.1016/j.aqpro.2015.02.058. URL <https://www.sciencedirect.com/science/article/pii/S2214241X15000590>.
- M. Mohammadi, A. Sharifi, M. Hosseingholizadeh, and A. Tariq. Detection of oil pollution using SAR and optical remote sensing imagery: A case study of the persian gulf. 49(10):2377–2385, 2021. ISSN 0974-3006. doi: 10.1007/s12524-021-01399-2. URL <https://doi.org/10.1007/s12524-021-01399-2>.
- S.-H. Park, H.-S. Jung, M.-J. Lee, W.-J. Lee, and M.-J. Cho. Oil spill detection from planetscope satellite image: Application to oil spill accident near ras al zour area, kuwait in august 2017. *Journal of Coastal Research*, pages 251–260, 2019. ISSN 07490208, 15515036. URL <https://www.jstor.org/stable/26778961>.
- A. Press. Kuwait battles oil spill in persian gulf waters — cbc news, Aug 2017. URL <https://www.cbc.ca/news/world/kuwait-battles-oil-spill-in-persian-gulf-waters-1.4245702>.
- S. Rajendran, P. Vethamony, F. N. Sadooni, H. A.-S. Al-Kuwari, J. A. Al-Khayat, H. Govil, and S. Nasir. Sentinel-2 image transformation methods for mapping oil spill – a case study with wakashio oil spill in the indian ocean, off mauritius. 8:101327, 2021a. ISSN 2215-0161. doi: 10.1016/j.mex.2021.101327. URL <https://www.sciencedirect.com/science/article/pii/S2215016121001205>.
- S. Rajendran, P. Vethamony, F. N. Sadooni, H. A.-S. Al-Kuwari, J. A. Al-Khayat, H. Govil, and S. Nasir. Sentinel-2 image transformation methods for mapping oil spill – a case study with wakashio oil spill in the indian ocean, off mauritius. 8:101327, 2021b. ISSN 2215-0161. doi: 10.1016/j.mex.2021.101327. URL <https://www.sciencedirect.com/science/article/pii/S2215016121001205>.
- D. A. Renegar, P. A. Schuler, A. H. Knap, and R. E. Dodge. TRopical oil pollution investigations in coastal systems [TROPICS]: A synopsis of impacts and recovery. 181: 113880, 2022. ISSN 0025-326X. doi: 10.1016/j.marpolbul.2022.113880. URL <https://www.sciencedirect.com/science/article/pii/S0025326X22005628>.

- S. S. Sardi, M. A. Qurban, W. Li, K. P. Kadinjappalli, P. K. Manikandan, M. M. Hariri, B. S. Tawabini, A. B. Khalil, and H. El-Askary. Assessment of areas environmentally sensitive to oil spills in the western arabian gulf, saudi arabia, for planning and undertaking an effective response. 150:110588, 2020. ISSN 0025-326X. doi: 10.1016/j.marpolbul.2019.110588. URL <https://www.sciencedirect.com/science/article/pii/S0025326X19307362>.
- B. Schaeffer, P. Whitman, R. Conmy, W. Salls, M. Coffey, D. Graybill, and M. C. Lebrasse. Potential for commercial planetscope satellites in oil response monitoring. *Marine Pollution Bulletin*, 183:114077, 2022. ISSN 0025-326X. doi: <https://doi.org/10.1016/j.marpolbul.2022.114077>. URL <https://www.sciencedirect.com/science/article/pii/S0025326X22007597>.
- C. Sheppard, M. Al-Husiani, F. Al-Jamali, F. Al-Yamani, R. Baldwin, J. Bishop, F. Benzonni, E. Dutrieux, N. K. Dulvy, S. R. V. Durvasula, D. A. Jones, R. Loughland, D. Medio, M. Nithyanandan, G. M. Pilling, I. Polikarpov, A. R. G. Price, S. Purkis, B. Riegl, M. Saburova, K. S. Namin, O. Taylor, S. Wilson, and K. Zainal. The gulf: A young sea in decline. 60(1):13–38, 2010. ISSN 0025-326X. doi: 10.1016/j.marpolbul.2009.10.017. URL <https://www.sciencedirect.com/science/article/pii/S0025326X09004585>.
- A. Solberg, G. Storvik, R. Solberg, and E. Volden. Automatic detection of oil spills in ers sar images. *IEEE Transactions on Geoscience and Remote Sensing*, 37(4):1916–1924, 1999. doi: 10.1109/36.774704.
- A. H. S. Solberg, C. Brekke, and P. O. Husoy. Oil spill detection in radarsat and envisat sar images. *IEEE Transactions on Geoscience and Remote Sensing*, 45(3):746–755, 2007. doi: 10.1109/TGRS.2006.887019.
- A. Taravat, D. Latini, and F. Del Frate. Fully automatic dark-spot detection from sar imagery with the combination of nonadaptive weibull multiplicative model and pulse-coupled neural networks. *IEEE Transactions on Geoscience and Remote Sensing*, 52(5):2427–2435, 2014. doi: 10.1109/TGRS.2013.2261076.
- K. Vankayalapati, H. P. Dasari, S. Langodan, S. El Mohtar, S. Sanikommu, K. Asfahani, S. Desamsetti, and I. Hoteit. Multi-mission satellite detection and tracking of october 2019 sabiti oil spill in the red sea. 15(1):38. ISSN 2072-4292. doi: 10.3390/rs15010038. URL <https://www.mdpi.com/2072-4292/15/1/38>. Number: 1 Publisher: Multidisciplinary Digital Publishing Institute.

- J. Yang, J. Wan, Y. Ma, J. Zhang, and Y. Hu. Characterization analysis and identification of common marine oil spill types using hyperspectral remote sensing. 41(18):7163–7185, 2020. ISSN 0143-1161. doi: 10.1080/01431161.2020.1754496. URL <https://doi.org/10.1080/01431161.2020.1754496>. Publisher: Taylor & Francis eprint: <https://doi.org/10.1080/01431161.2020.1754496>.
- J. Zhao, M. Temimi, H. Ghedira, and C. Hu. Exploring the potential of optical remote sensing for oil spill detection in shallow coastal waters-a case study in the arabian gulf. *Opt. Express*, 22(11):13755–13772, Jun 2014. doi: 10.1364/OE.22.013755. URL <https://opg.optica.org/oe/abstract.cfm?URI=oe-22-11-13755>.